THE JOURNAL OF PHYSICAL CHEMISTRY C

Article

Cite This: J. Phys. Chem. C 2019, 123, 12382−12389

pubs.acs.org/JPCC

The Pressure Gap for Thiols: Methanethiol Self-Assembly on Au(111) from Vacuum to 1 bar

Rik V. Mom,[*,†,●,^] Sigismund T. A. G. Melissen,[‡,●,^] Philippe Sautet,[§,∥] Joost W. M. Frenken,[⊥] Stephan N. Steinmann,[*,#] and Irene M. N. Groot[†,∇]

[†]Huygens-Kamerlingh Onnes Laboratory, Leiden University, Niels Bohrweg 2, 2333 CA Leiden, The Netherlands

[‡]Université de Lyon, Université Claude Bernard Lyon 1, CNRS, Institut Lumière Matière, F-69622 Lyon, France

[§]Department of Chemical and Biomolecular Engineering and [∥]Department of Chemistry and Biochemistry , University of California at Los Angeles, Los Angeles, California 90095, United States

[⊥]Advanced Research Center for Nanolithography, Science Park 110, 1098 XG Amsterdam, The Netherlands

[#]Université de Lyon, Ens de Lyon, CNRS UMR 5182, Université Claude Bernard Lyon 1, Laboratoire de Chimie, F-69342, Lyon, France

[∇]Leiden Institute of Chemistry, Leiden University, Einsteinweg 55, 2333 CC Leiden, The Netherlands

Supporting Information

ABSTRACT: Functionalizing noble metal surfaces with (bio)-organic molecules is a vibrant field of research, with key applications in medicine, catalysis, and molecular electronics. Control over the molecular self-assembly is essential to creating functional devices. Here, we exploit our high-pressure, high-temperature scanning tunneling microscope (STM) to relate the effects of controllable parameters (temperature and pressure) to atomic-scale assembly mechanisms. Using methanethiol self-assembly on Au(111) as a model system, we monitor the formation and assembly of the ubiquitous $(CH_3S)_2Au$ "staple" motif into row structures at pressures of up to 1 bar. We observe a pressure-induced transition from the usual 1/3 monolayer (ML) saturation coverage in vacuum to 3/8 ML at 1 bar, thus providing the first evidence for a pressure gap effect for thiol adsorption. Complementing our experiments, we employed dispersion-corrected density functional theory computations to model the formed surface adlayers, corresponding STM images, and underlying equilibrium thermodynamics.

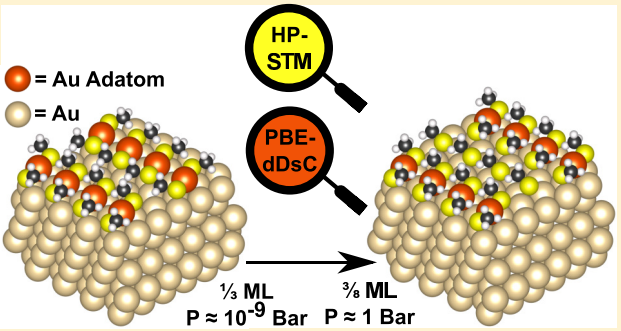

1. INTRODUCTION

Thiol molecules on gold provide a scaffold to which virtually any organic molecule can be attached. While the sulfur headgroup ensures firm bonding to the gold substrate, the tail of the molecule can be functionalized with reactive groups that allow bonding to other molecules. In this way, complex structures can be created that specifically target biomolecules in medical science (cf. refs 17−21 in ref 1), enhance (chiral) selectivity in catalysis,[2] or provide unique electrical properties for molecular electronics.[3] For these applications, control over the thiol surface structure is essential. At first glance, this task appears to be simple: thiol molecules on gold tend to form crystalline self-assembled monolayers (SAMs) (an overview of acronyms used in this manuscript is provided before the bibliography), even at moderate temperatures.[1,2,4,5] However, the coexistence of multiple phases is difficult to prevent, particularly for larger thiol molecules.[4,6,7]

To find handles to tune the thiol overlayer structure, intimate knowledge of the bonding behavior and kinetics during self-assembly is required. A wide variety of microscopy,[4,7−14] spectroscopy,[15−20] and scattering[21] techniques have been applied to these systems, complemented by theoretical modeling.[1,19,21−23] It was found that following thiol adsorption the S−H bond of the headgroup is broken and H_2 is formed as a byproduct. While formally a thiyl radical is formed in this process, the adsorbate is usually called a "thiolate" or thiol, despite having neither a net negative charge nor a hydrogen atom. Thiolates have such an affinity for gold that Au atoms are extracted[24] from the close-packed terraces to be incorporated in the thiol overlayer structure.[1,9−11,21] It was established that the Au adatoms are bound by two thiol molecules, forming thiol−Au−thiol "staples".[1,4,10,21] In the final step of overlayer formation, the staples self-assemble into crystalline phases.

While the fundamental studies have thus identified the key formation steps and structural elements in self-assembled monolayers, most of them were conducted under vacuum conditions, whereas elevated pressure or liquid-phase SAM

Received: April 1, 2019
Revised: April 24, 2019
Published: April 25, 2019

DOI: 10.1021/acs.jpcc.9b03045
J. Phys. Chem. C 2019, 123, 12382−12389

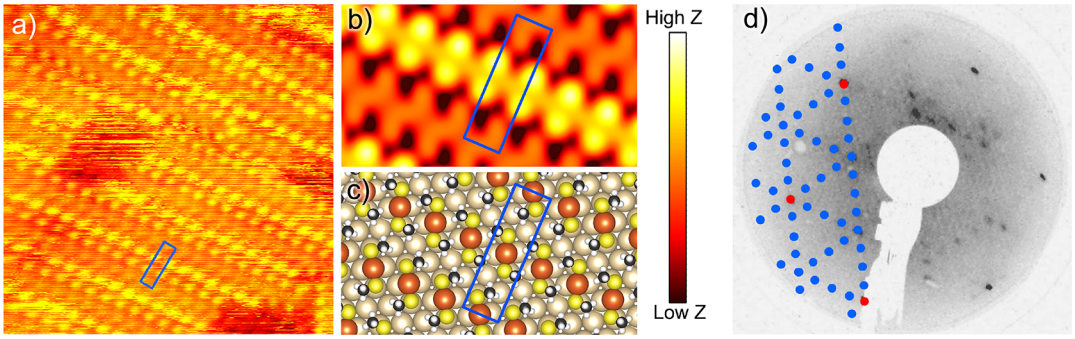

Figure 1. Adsorption structure of methanethiolate on Au(111) after saturation in vacuum. (a) $6 \times \sqrt{3}$ methanethiolate SAM obtained after 21 h of dosing ($P_{CH_3SH} = 10^{-6}$ mbar, $P_{H_2} = 10^{-10}$ mbar) at room temperature, 10 × 10 nm^2, $U_s = -1.0$ V, $I_t = 150$ pA. Corrugation in the SAM structure is 0.05 nm, as determined from line scans perpendicular to the row direction. Note that the corrugation in STM images is strongly affected by the tip apex structure and might therefore change from image to image. (b) Simulated STM image (−1 V, 500 pA, corrugation 0.07 nm) for the structure in panel a. (c) The corresponding ball model. Atoms in orange, Au adatoms; gold: lattice Au atoms; yellow, S; black, C; and white, H. (d) LEED pattern showing the (1 × 1) Au lattice (red dots) and the $6 \times \sqrt{3}$ SAM overlayer (blue dots, three domain orientations).

growth is much more attractive in practical applications. For several metal−adsorbate systems, it was shown that such a "pressure gap" can have a significant effect on the behavior of adsorbates.[25−27] Here, we have studied methanethiol adsorption on Au(111) on both sides of the pressure gap: with our high-pressure, high-temperature scanning tunneling microscope (STM),[28] we assess the SAM structures formed at pressures ranging from ultrahigh vacuum (UHV) to 1 bar at temperatures of up to 523 K. Through the variation of temperature and pressure, we relate control parameters to the kinetic and thermodynamic factors that affect the SAM ordering and crystal structure. Our data is compared to extensive density functional theory (DFT) modeling, taking into account the effects of entropy and Van der Waals (VdW) interactions. This methodology allows us to thoroughly characterize SAM formation on the thermodynamic and kinetic levels under relevant conditions and characterize the highest-ever reported thiol coverage, here achieved at 1 bar and 383 K.

2. METHODS

2.1. Experimental Methods. *2.1.1. Setup Description.* Microscopy at elevated pressure and temperature constitutes a technical challenge. To enable our studies at pressures of up to 1 bar, we used the ReactorSTM developed in our group.[28] In short, this system allows for the preparation and characterization in UHV as well as high-pressure STM studies using a 0.5 mL flow cell inside the vacuum system. Gases are introduced into the flow reactor from a dedicated gas supply system, which allows for accurate control over the gas composition, flow, and pressure. All components that are in contact with the gas environment are made of corrosion-resistant steel alloys, glass, poly(ether imide), or Kalrez to prevent degradation upon exposure to reactive gases such as CH_3SH. The use of PtIr STM tips prevents tip degradation during the measurements. Nevertheless, frequent changes in imaging quality due to the adsorption/desorption of gas molecules on the tip apex cannot be avoided.

In addition to the scanning tunneling microscope, the system is equipped with a low-energy electron diffraction (LEED) apparatus (Omicron) and an X-ray photoelectron spectrometer (SPECS Phoibos). A quadrupole mass spectrometer was used to verify the purity of the employed gases.

2.1.2. Experimental Procedures. The Au(111) sample (Surface Preparation Laboratories)[29] was cleaned by cycles of 1 keV Ar^+ bombardment and annealing at 900 K. For the formation of methanethiolate SAMs under UHV conditions, CH_3SH (N1.8, Westfalen AG, containing approximately 2 vol % dimethyldisulfide (DMDS)[30]) was dosed via capillaries close to the sample surface. All UHV dosing was performed at room temperature.

Prior to high-pressure experiments, all gas lines were flushed with argon for at least 30 min. To start the high-pressure exposure, the reactor was slowly pressurized in argon or nitrogen before heating to the desired temperature. To minimize the thermal drift in the microscope, the system was allowed an equilibration period of approximately 90 min. Whenever expedient, imaging was started before introducing CH_3SH so that the surface dynamics upon exposure could be monitored.

2.2. Computational Methods. *2.2.1. Structure Determination.* Electronic structure computations were performed using the Projector Augmented-Wave (PAW) formalism to account for the ion−electron interaction[31] as implemented in Vienna *Ab Initio* Simulation Package (VASP) 5.4.1.[32−35] The wave function was expanded in a plane wave basis set characterized by a cutoff energy of 400 eV. Generalized Gradient Approximation (GGA) functional Perdew−Burke−Ernzerhof (PBE)[36,37] was used, in combination with the "dDsC" dispersion correction,[38] which has been shown to be accurate for adsorption energies on Pt(111)[39] and has been successfully applied to the adsorption of pyridine on Au(111).[40] Second-order Methfessel−Paxton electron smearing (width of 0.2 eV) was applied to metallic surfaces. Ionic relaxations were performed using a conjugate-gradient algorithm to a maximum gradient below 0.05 eV/Å, with wave functions converged to 10^{-5}. A Monkhorst−Pack K-point sampling[41] of at least 3 × 3 × 1 was applied to all surfaces in order to converge the adsorption energies. A primitive unit cell parameter of 2.928 Å was specified, corresponding to the optimized Au bulk unit cell of 4.141 Å. A vacuum layer of 10 Å was used to separate the vertical repetitions of the slabs.

For the STM simulations, the unit cell was replicated because our version of the code does not support K-point sampling. We used five full metallic layers, of which the three bottom layers were fixed in their bulk positions. Note that the

DOI: 10.1021/acs.jpcc.9b03045
J. Phys. Chem. C 2019, 123, 12382−12389

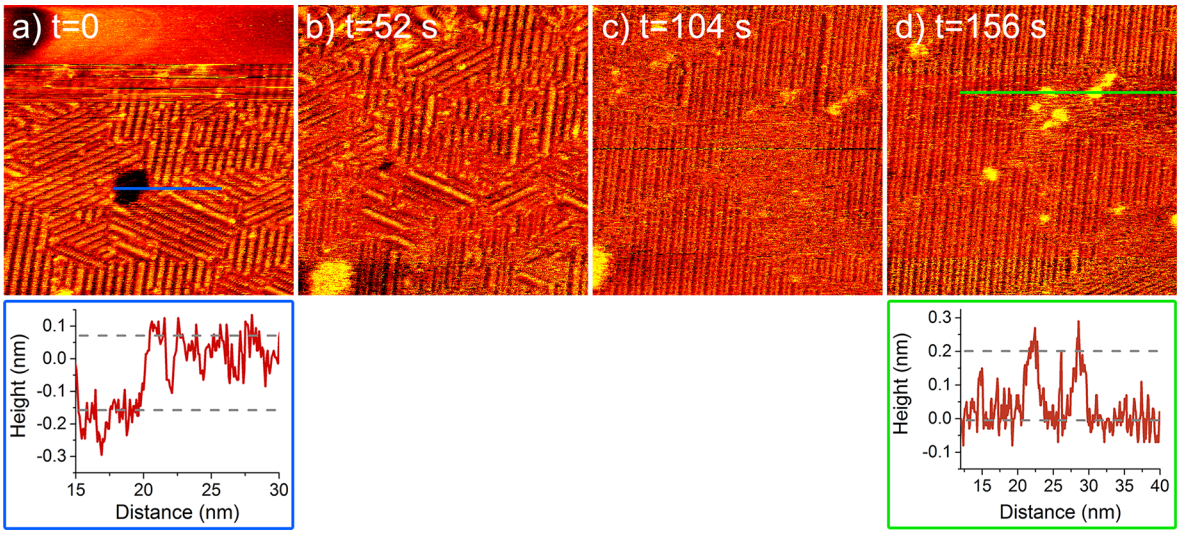

Figure 2. Structural transition from the 1/3 ML phase to a high-pressure structure after introducing 1 bar CH_3SH at 383 K. Imaging parameters for a–d: 40 × 40 nm^2, U_s = −1 V, I_t = 150 pA. Height lines identify an Au vacancy island (blue) and Au adatom islands (green).

herringbone reconstruction[42] was neglected in our computations.

STM images were simulated by the approach of Tersoff and Hamann,[43−45] at a bias voltage of −1 V and a current of 10^{-9} A (unless stated otherwise) on the basis of the PBE band structure at the Γ point of super cells.

2.2.2. Thermodynamics. Frequency computations were performed to estimate zero-point energies and vibrational entropy corrections within the harmonic oscillator approximation. For these computations, all gold atoms were kept frozen. All frequencies were real and above 40 cm^{-1}. Adsorption energies for structures with gold adatoms are referenced to the Au(111) surface and Au atoms from the bulk. Adsorption free energies were calculated on the basis of the following reaction:

$$CH_3SH + Au(111) \rightleftharpoons CH_3S{-}Au(111) + \frac{1}{2}H_2 \quad (1)$$

When estimating thermal contributions to the Gibbs energy, we made the usual assumptions of harmonic oscillators for vibrations. For gas-phase molecules, we also invoke the rigid-rotor approximation and the Sackur−Tetrode equation for the rotational and translational contributions, respectively. The energy required to bring one Au atom from the bulk onto the Au(111) surface is on the order of 0.7 eV. To allow for a wider comparison of our data to the literature, we also provide data for the calculation of adsorption energies in a DMDS gas atmosphere in Table S1 in the SI.

3. RESULTS AND DISCUSSION

We investigated the effect of pressure on the structure of the methanethiolate overlayer using controlled dosing experiments in vacuum (10^{-6} mbar) and at 1 bar. For the vacuum case, several saturation structures have already been identified in the literature,[11,46,47] each with 1/3 monolayer (ML) coverage. In our case, the surface is saturated with a striped phase with a $6 \times \sqrt{3}$ unit cell (Figure 1) after several hours of 10^{-6} mbar CH_3SH exposure at room temperature. (See Figure S1 in the ESI for the structural evolution during the self-assembly.) Similar striped phases have been reported in the literature, although ordering of the stripes into densely packed domains was never observed.[10,11,46,48] We point out that exchange reactions with strong-binding impurities from the gas feed, such as ethanethiol, can be excluded because the stripe motifs were already observed in the initial stages of self-assembly (90 min, Figure S1a in the SI). The stripes have been identified as rows of thiol−Au−thiol staples, which can appear in several structural isomers. Our DFT simulations (SI section S3.3) of the staple structures indicate that the inclusion of Au adatoms in the SAMs indeed improves the Au−S interaction (∼0.25 eV per thiol), while the staple packing and isomeric form are determined by the methyl−methyl repulsion (up to ∼0.4 eV per thiol). Our computations indicate that several isomers have a very comparable formation energy, explaining why multiple phases have been observed in the literature.[10,11,46,47] Indeed, depending on the tip's state and its interactions with the surface, the SAM was sometimes observed as a $3 \times \sqrt{3}$ line structure (Figure S2 in the SI).

To identify the experimentally observed structure observed in Figure 1a, we used simulated STM images. The simulated STM image in Figure 1b (with the corresponding ball model in Figure 1c) shows the best agreement with the experimental image (Figure 1a), accurately reproducing the alternating brightness in the line structure, in contrast to the simulations of other models (Figure S3 in the SI). Although the fine structure is not fully resolved in the experimental image, the bright protrusions (∼0.1−0.2 Å) originating from half of the methyl groups show the same rectangular pattern in both the experimental and simulated images. With this good agreement, the structure in Figure 1c is assigned to the vacuum saturation coverage structure shown in Figure 1a. Similar to the other phases observed in the literature,[11,46,47] this structure has a coverage of 1/3 ML.

To investigate if a coverage higher than $\frac{1}{3}$ ML can be obtained at elevated pressure, we imaged the Au(111) surface in 1 bar CH_3SH at several temperatures. Figure 2 shows the structural evolution of the SAM directly after changing the partial pressure of CH_3SH from trace levels to 1 bar at 383 K. The initial vacuum saturation-coverage phase (which appears as a $3 \times \sqrt{3}$ structure in Figure 2a) is quickly replaced by a new phase with paired lines. The new structure is stable only under

DOI: 10.1021/acs.jpcc.9b03045
J. Phys. Chem. C 2019, 123, 12382−12389

high-pressure conditions: when the partial pressure of CH_3SH is brought back down to trace levels, the $3 \times \sqrt{3}$ structure is recovered (Figure 3). Thus, it is clear that the CH_3SH pressure can be used to drive a reversible phase transition.

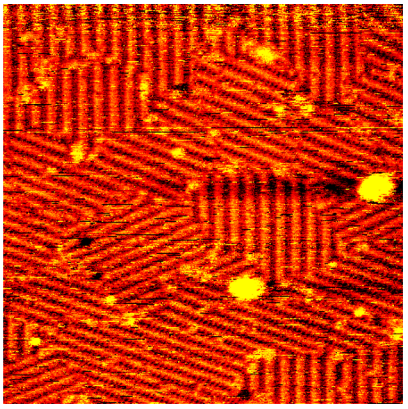

Figure 3. Reversibility of the high-pressure phase transition following the decrease in the CH_3SH pressure to trace levels (in 1 bar N_2), 383 K. Imaging parameters: 35×35 nm^2, $U_s = -1$ V, $I_t = 150$ pA.

For such a pressure-driven transition, there is an increase in the adsorbate coverage.[25−27] To establish which CH_3SH coverage is achieved, we first determined the unit cell shape under high-pressure conditions. This is a challenge because the drift in the microscope at high pressure and temperature causes some image distortion. Using large-scale images with a high tip speed, we minimized the effect of drift and established that the unit cell has the same orientation as in the 1/3 ML case. The periodicity perpendicular to the stripes is four Au spacings. The periodicity along the stripe direction was determined to be $\sqrt{3}$ Au spacing using Figure 4c. Thus, we arrive at a $4 \times \sqrt{3}$ unit cell. The highest thiol coverage that allows for reasonable orientation of the methyl groups in this unit cell is 3/8 ML.

A closer inspection of the images in Figure 2 reveals that the denser packing of CH_3SH is enabled by the release of Au from the SAM: the vacancy island in Figure 2a is filled (Figure 2c), and Au adatom islands (Figure 2b−d) are formed. We quantified the vacancy island coverage within a few minutes after the transition to high pressure in several fresh areas on wide terraces (e.g., Figure 4a), thus minimizing the influence of the tip and step edges as sinks for the adatoms. We find that the amount of released Au is large and strongly fluctuating: 0.22 ± 0.07 ML. This amount is in the same range as the 0.17 ML that is contained in the perfect 1/3 ML structure. On the basis of this, one could hypothesize that the high-pressure phase does not contain Au adatoms. However, our DFT computations show that 3/8 ML structures without Au adatoms are more than 0.2 eV less stable per adsorbed thiol (i.e., more than 0.6 eV for the 3/8 ML unit cell) than their Au-containing counterparts. (See Table S2 in the SI for the most stable one out of seven tested configurations.) Furthermore, the large spread in Au adatom island coverage suggests that there is a second source of Au atoms that shows more fluctuation than a pure crystalline phase. We suggest that the domain boundaries in the SAM are this second source. Indeed, Figure 3 shows that small Au clusters can be generated at the domain boundaries following dynamic situations such as phase transitions or the initial formation of the SAM.

On the basis of the discussion above, we considered candidate high-pressure structures with a $4 \times \sqrt{3}$ unit cell, 3/8 ML CH_3SH coverage, and 1/8 ML Au adatom coverage (Figure S4 in the SI). Following the structural motifs identified in the literature, these contain a mixture of "staples" and bridge-bonded thiolates.[10,11,21,46,47,49] Again, we find several isomers with similar formation energy, necessitating further distinction using STM simulations. The simulation in Figure 4d, based on the structure in Figure 4e, reproduces the bright paired rows observed in the experiment (Figure 4c). Note that the row spacing in the experimental image (Figure 4c) is somewhat stretched by the drift in the microscope under high-pressure, high-temperature conditions. The "bright" row pairs, also clearly observed for the low-pressure case (Figure 1a,b), characterize the trans-staple motif for which the methyl groups are equidistant to (1) the Au adatom to which they are covalently bound through S and (2) a neighboring Au adatom. The thiolates between the staples, which are bridge-bonded with a tendency toward the hcp site, appear dark in both the experimental and simulated image. The alignment of the bridge-bonded thiolates with respect to the staples is difficult to determine from the experimental image, but the STM simulations allow differentiation (cf. Figure S4) between very similar structures. On the basis of this agreement, we identify the high-pressure structure with the structure shown in Figure 4e.

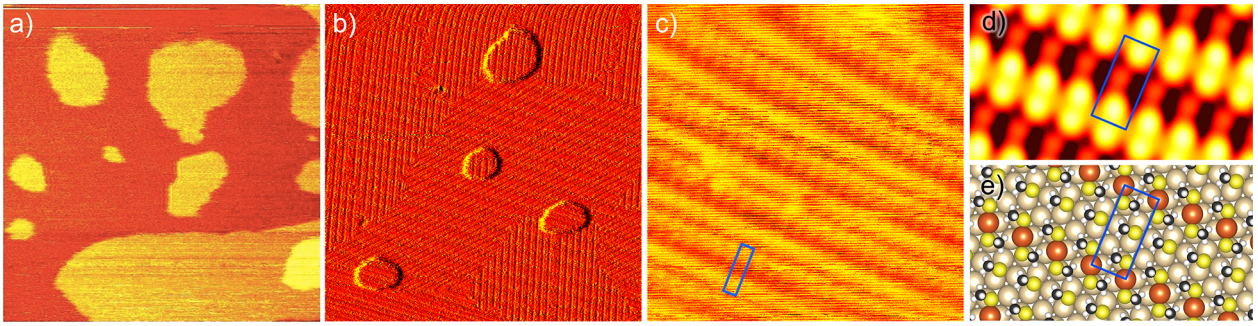

Figure 4. Structure of methanethiolate SAM at 1 bar (P_{CH_3SH} = 1000 mbar, P_{H_2} = 0.35 mbar), 383 K. (a) Au adatom islands shortly after the transition from trace levels to 1 bar CH_3SH (80×80 nm^2, $U_s = -0.2$ V, $I_t = 120$ pA). (b) SAM structure on adatom islands. The STM image was differentiated to visualize the SAM structure on both the terrace and the adatom islands (80 nm × 80 nm, $U_s = -0.1$ V, $I_t = 800$ pA). (c) Details of the SAM structure, 10×10 nm^2, $U_s = -0.1$ V, $I_t = 800$ pA. Corrugation in SAM structure: 0.02 nm. (d) Simulated STM image (−1 V, 500 pA, corrugation 0.08 nm) for the structure in panel c. (e) The corresponding ball model.

DOI: 10.1021/acs.jpcc.9b03045
J. Phys. Chem. C 2019, 123, 12382−12389

With a coverage of 3/8 ML, this is the most densely packed SAM reported in the literature, evidencing the existence of a pressure gap for thiol adsorption. Note that Mehring et al.[14] observed a similar $4 \times \sqrt{3}$ structure after the exposure of Au(111) to a 1 mM DMDS/ethanol solution for several hours. They suggested a structure with only 1/4 ML coverage. While the competition between thiol and solvent adsorption might have resulted in such a structure under their conditions, our observation of a pressure-induced transition provides clear evidence of a structure with a coverage higher than that obtained in UHV.

To relate the observations in Figures 1a and 4c to equilibrium thermodynamics, we calculated the corresponding adsorption free energies using

$$\Delta G_{ads} = \Delta E_{ads} + \Delta ZPE_{ads} + \delta H^{T}_{ads} - T\Delta S_{ads} \quad (2)$$

where E_{ads} is the sum of electronic energies E_{PBE} and E_{dDsC}, ZPE refers to the zero-point energies, δH^{T} refers to the thermal correction to the enthalpy, and S refers to the entropy. The vibrational contributions of the SAMs were taken into account in the calculation (details in the Thermodynamics section) .

Figure 5 shows that both the 1/3 ML and 3/8 ML structures are thermodynamically predicted to be at least metastable at the respective conditions under which they were experimentally observed. (See Section 3.4 in the ESI for a discussion on relative stability.) Second, the decomposition shows that neither the change in ZPE, nor in the enthalpy corrections contributes significantly to the adsorption free energy. The adsorption entropy, however, does significantly offset ΔE_{ads}. Because the entropic contribution to the free energy is strongly dependent on temperature and pressure, this shows that the applied conditions strongly influence the stability of the SAM structures. The pressure increase from 10^{-6} mbar to 1 bar lowers the entropic penalty for adsorption according to

$$\Delta G = k_B T \ln(p/p') \quad (3)$$

Despite the 90 K temperature difference between Figures 1a and 4c, Figure 5 shows that the pressure increase dominates and thus lowers the entropy cost, providing a stabilizing force for higher thiol coverage. A further temperature increase should undo this stabilizing effect, however, and can even lead to desorption of the SAM. Figure 6a shows that desorption occurs at 523 K, where only the (1×1) Au(111) lattice is visible despite the high CH_3SH pressure. Note that the observation of the (1×1) lattice does not imply a completely empty surface because a small amount of thiolates could be obscured from STM observation as a result of their fast motion. Indeed, the absence of the heringbone reconstruction indicates that some thiolates remain on the surface. Nonetheless, the coverage decrease demonstrates that the entropy in the gas phase outcompetes both the pressure and the adsorption energy under these conditions.

At lower temperatures, adsorption kinetics play a dominant role. As can be seen in Figure 6b, room-temperature exposure at 1 bar results in a very poorly ordered structure, containing $3\times\sqrt{3}$ line structures similar to those observed after UHV exposure. The lack of ordering establishes that thiol adsorption, S−H bond dissociation, and staple formation proceed significantly faster than the ordering process. Note that the SAM structure did not proceed to the $4\times\sqrt{3}$ phase even though the thermodynamic driving force is higher than in the experiment at 383 K (Figure 4c). Clearly, the hampered diffusion at 1/3 ML coverage prevents the insertion of more thiol molecules into the SAM.

On the basis of our observations and simulations for various conditions, Figure 7 shows an overview of the relation between the applied conditions and the observed structure. One distinguishes conditions where the structure is determined by kinetics and others that lead to thermodynamic control. The kinetically controlled region tends toward lower coverage and disorder and originates from the mismatch between the (fast) staple formation rate and the (slower) staple ordering rate. The

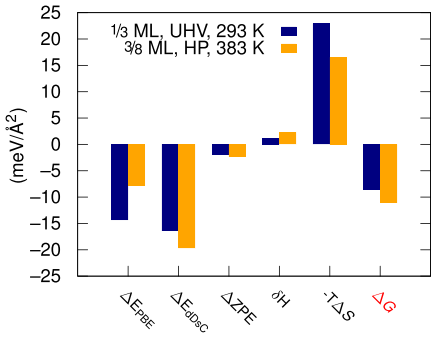

Figure 5. Contributions to the surface free energy according to eq 2 for 1/3 ML under UHV, 293 K and 3/8 ML under HP, 383 K conditions.

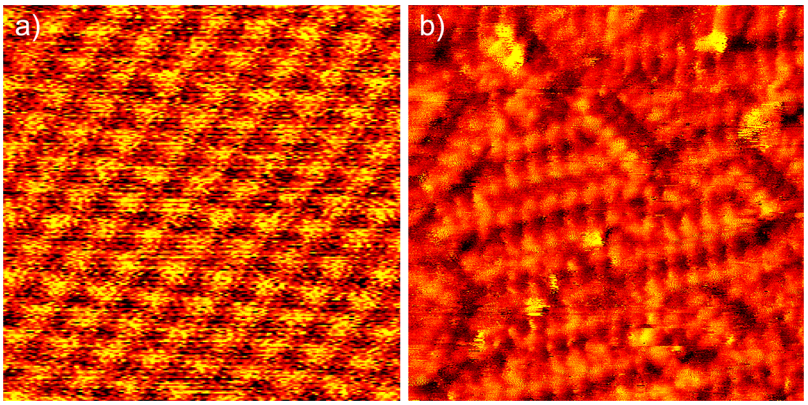

Figure 6. Effect of temperature on CH_3SH adsorption at 1 bar. (a) Empty Au(111) surface imaged at 523 K (2.5 × 2.5 nm^2, U_s = −0.3 V, I_t = 520 pA). (b) Kinetically hindered CH_3SH adsorption at room temperature (10 × 10 nm^2, U_s = −0.3 V, I_t = 520 pA).

DOI: 10.1021/acs.jpcc.9b03045
J. Phys. Chem. C 2019, 123, 12382−12389

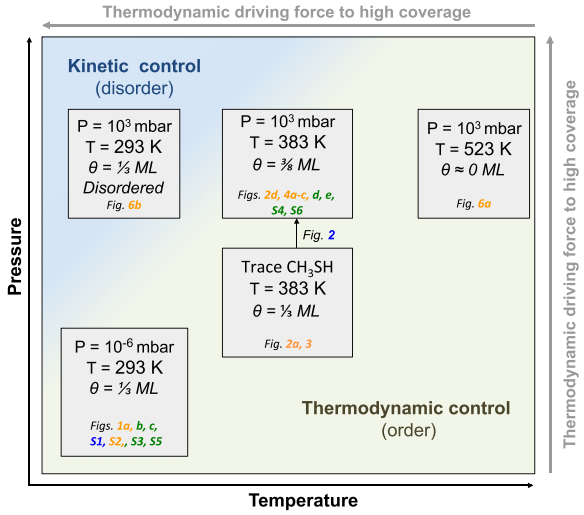

Figure 7. Conceptualization of thermodynamic and kinetic factors determining SAM structures. The different structures and transformations are linked to the figures in this article. (Blue) SAM formation process. (Green) Theoretical analysis. (Orange) Equilibrium/kinetically stable SAMs.

rate mismatch is largest for low temperature (Figure 6b vs Figure 4c) and/or high pressure (Figure 6b vs Figure 1a).

At low pressure and/or high temperature, thermodynamic control takes over. Our computations show that the balance of the Au−S interaction, the van der Waals interactions, and the gas-phase entropy determines the relative stability of the various SAM structures. Through the gas-phase entropy, higher pressure favors higher coverage (Figure 4c vs Figure 1a), while higher temperature favors lower coverage (Figure 4c vs Figure 6). Note, however, that our computations show that several structures with the same coverage are energetically very close (Figures S3−S6 in the SI). Thus, subtle factors such as the energetic cost of defect formation (impurities, step edges, and domain boundaries) may also determine which structure is observed.

4. CONCLUSIONS

We have identified the key thermodynamic and kinetic factors that control methanethiolate SAM formation and have related these factors to the applied temperature and pressure. Most importantly, we have shown that, beside affecting the SAM order, the dosing pressure can induce a phase transition to the newly revealed 3/8 ML phase. Such pressure- or concentration-induced transitions will likely also occur for functionalized SAMs, for which repulsive tail−tail interactions may exist, which are in competition with optimizing the Au−thiol interaction.[50] We therefore expect that the fundamental insights gained here will apply to a wide range of technologically relevant SAMs and provide handles for their controlled growth.

■ ASSOCIATED CONTENT

Supporting Information

The Supporting Information is available free of charge on the ACS Publications website at DOI: 10.1021/acs.jpcc.9b03045.

Additional STM data and an extensive theoretical analysis based on DFT energetics and simulated STM images; an expression for the equilibrium hydrogen pressure in the reactor; the geometries of all structures in the CONTCAR format; and the energies and entropies computed for the ab initio thermodynamics modeling are provided (PDF)

■ AUTHOR INFORMATION

Corresponding Authors

*E-mail: mom@physics.leidenuniv.nl. Phone: +49.30.8413.4640. Fax: +49.30.8413.4401.

*E-mail: stephan.steinmann@ens-lyon.fr. Phone: + 33.4.72.72.81.55. Fax: + 33.4.72.72.88.60.

ORCID

Rik V. Mom: 0000-0002-5111-5591

Sigismund T. A. G. Melissen: 0000-0002-8728-9382

Philippe Sautet: 0000-0002-8444-3348

Stephan N. Steinmann: 0000-0002-2777-356X

Irene M. N. Groot: 0000-0001-9747-3522

Present Address

•Fritz-Haber Institut der Max-Planck-Gesellschaft, Faradayweg 4-6, 14195 Berlin, Germany

Author Contributions

^These authors contributed equally to this article.

Notes

The authors declare no competing financial interest.

■ ACKNOWLEDGMENTS

This project was financially supported by a Dutch SmartMix grant and by NIMIC partner organizations through NIMIC, a public−private partnership. I.M.N.G. acknowledges the Dutch organization for scientific research (NWO-STW) for her Veni fellowship. S.N.S. and S.T.A.G.M. gratefully acknowledge the computational resources provided by the Pôle Scientifique de Modélisation Numérique (PSMN) at ENS Lyon. S.N.S. is grateful to N. Lorente and T. Jiang for sharing code and scripts, respectively.

■ LIST OF ALPHABETICALLY ORDERED ACRONYMS

DFT density functional theory; DMDS dimethyldisulfide; GGA generalized gradient approximation; hcp hexagonally close packed; LEED low-energy electron diffraction; ML monolayer; PAW projector-augmented wave; PBE Perdew−Burke−Ernzerhof; PES potential energy surface; SAM self-assembled monolayers; STM scanning tunneling microscope; UHV ultrahigh vacuum; VASP Vienna ab initio simulation package; vdW van der Waals; ZPE zero-point energy

■ REFERENCES

(1) Häkkinen, H. The Gold-Sulfur Interface at the Nanoscale. *Nat. Chem.* **2012**, *4*, 443−455.

(2) Bürgi, T. Properties of the Gold-Sulphur Interface: from Self-Assembled Monolayers to Clusters. *Nanoscale* **2015**, *7*, 15553−15567.

(3) Tour, J. M. Molecular Electronics. Synthesis and Testing of Components. *Acc. Chem. Res.* **2000**, *33*, 791−804.

(4) Pensa, E.; Cortés, E.; Corthey, G.; Carro, P.; Vericat, C.; Fonticelli, M. H.; Benitez, G.; Rubert, A. A.; Salvarezza, R. C. The Chemistry of the Sulfur-Gold Interface: In Search of a Unified Model. *Acc. Chem. Res.* **2012**, *45*, 1183−1192.

(5) Poirier, G. E. Characterization of Organosulfur Molecular Monolayers on Au (111) Using Scanning Tunneling Microscopy. *Chem. Rev.* **1997**, *97*, 1117−1128.

(6) Sotthewes, K.; Wu, H.; Kumar, A.; Vancso, G. J.; Schön, P. M.; Zandvliet, H. J. W. Molecular Dynamics and Energy Landscape of

Decanethiolates in Self-Assembled Monolayers on Au(111) Studied by Scanning Tunneling Microscopy. *Langmuir* **2013**, *29*, 3662−3667.
(7) Li, F.; Tang, L.; Zhou, W.; Guo, Q. Adsorption Site Determination for Au-Octanethiolate on Au(111). *Langmuir* **2010**, *26*, 9484−9490.
(8) Dishner, M. H.; Hemminger, J. C.; Feher, F. J. Direct Observation of Substrate Influence on Chemisorption of Methanethiol Adsorbed from the Gas Phase onto the Reconstructed Au(111) Surface. *Langmuir* **1997**, *13*, 2318−2322.
(9) Kautz, N. A.; Kandel, S. A. Alkanethiol Monolayers Contain Gold Adatoms, and Adatom Coverage Is Independent of Chain Length. *J. Phys. Chem. C* **2009**, *113*, 19286−19291.
(10) Maksymovych, P.; Sorescu, D. C.; Yates, J. T. Gold-Adatom-Mediated Bonding in Self-Assembled Short-Chain Alkanethiolate Species on the Au(111) Surface. *Phys. Rev. Lett.* **2006**, *97*, DOI: 10.1103/PhysRevLett.97.146103.
(11) Voznyy, O.; Dubowski, J. J.; Yates, J. T.; Maksymovych, P. The Role of Gold Adatoms and Stereochemistry in Self-Assembly of Methylthiolate on Au(111). *J. Am. Chem. Soc.* **2009**, *131*, 12989−12993.
(12) Zhang, J.; Chi, Q.; Ulstrup, J. Assembly Dynamics and Detailed Structure of 1-Propanethiol Monolayers on Au(111) Surfaces Observed Real Time by in situ STM. *Langmuir* **2006**, *22*, 6203−6213.
(13) Guo, Q.; Li, F. Self-Assembled Alkanethiol Monolayers on Gold Surfaces: Resolving the Complex Structure at the Interface by STM. *Phys. Chem. Chem. Phys.* **2014**, *16*, 19074−19090.
(14) Mehring, P.; Beimborn, A.; Westphal, C. The Structural Formation of Methylthiolate SAMs on Au(111) for Short Deposition Times from Solution. *Appl. Surf. Sci.* **2010**, *256*, 7265−7269.
(15) Roper, M. G.; Jones, R. G. Methylthiolate on Au(111): Adsorption and Desorption Kinetics. *Phys. Chem. Chem. Phys.* **2008**, *10*, 1336−1346.
(16) Kondoh, H.; Iwasaki, M.; Shimada, T.; Amemiya, K.; Yokoyama, T.; Ohta, T.; Shimomura, M.; Kono, S. Adsorption of Thiolates to Singly Coordinated Sites on Au(111) Evidenced by Photoelectron Diffraction. *Phys. Rev. Lett.* **2003**, *90*, 066102.
(17) Rousseau, R.; De Renzi, V.; Mazzarello, R.; Marchetto, D.; Biagi, R.; Scandolo, S.; del Pennino, U. Interfacial Electrostatics of Self-Assembled Monolayers of Alkane Thiolates on Au(111): Work Function Modification and Molecular Level Alignments. *J. Phys. Chem. B* **2006**, *110*, 10862−10872.
(18) Lavrich, D. J.; Wetterer, S. M.; Bernasek, S. L.; Scoles, G. Physisorption and Chemisorption of Alkanethiols and Alkyl Sulfides on Au (111). *J. Phys. Chem. B* **1998**, *102*, 3456−3465.
(19) Mazzarello, R.; Cossaro, A.; Verdini, A.; Rousseau, R.; Casalis, L.; Danisman, M. F.; Floreano, L.; Scandolo, S.; Morgante, A.; Scoles, G. Structure of a CH_3S Monolayer on Au(111) Solved by the Interplay between Molecular Dynamics Calculations and Diffraction Measurements. *Phys. Rev. Lett.* **2007**, *98*, 016102.
(20) Cheng, H.; Yang, L.; Jiang, Y.; Huang, Y.; Sun, Z.; Zhang, J.; Hu, T.; Pan, Z.; Pan, G.; Yao, T.; et al. Adsorption Kinetic Process of Thiol Ligands on Gold Nanocrystals. *Nanoscale* **2013**, *5*, 11795−11800.
(21) Cossaro, A.; Mazzarello, R.; Rousseau, R.; Casalis, L.; Verdini, A.; Kohlmeyer, A.; Floreano, L.; Scandolo, S.; Morgante, A.; Klein, M. L.; et al. X-ray Diffraction and Computation Yield the Structure of Alkanethiols on Gold(111). *Science* **2008**, *321*, 943−946.
(22) Andersson, M. P. Density Functional Theory with Modified Dispersion Correction for Metals Applied to Self-Assembled Monolayers of Thiols on Au(111). *J. Theor. Chem.* **2013**, *2013*, 327839.
(23) Jiang, D.-e.; Dai, S. Cis-trans Conversion of the CH_3S-Au-SCH_3 Complex on Au(111). *Phys. Chem. Chem. Phys.* **2009**, *11*, 8601−8605.
(24) Liao, W.-S.; Cheunkar, S.; Cao, H. H.; Bednar, H. R.; Weiss, P. S.; Andrews, A. M. Subtractive Patterning via Chemical Lift-Off Lithography. *Science* **2012**, *337*, 1517−1521.
(25) van Spronsen, M. A.; Frenken, J. W. M.; Groot, I. M. N. Observing the Oxidation of Platinum. *Nat. Commun.* **2017**, *8*, 429.
(26) Tao, F.; Dag, S.; Wang, L.-W.; Liu, Z.; Butcher, D.; Bluhm, H.; Salmeron, M.; Somorjai, G. Break-Up of Stepped Platinum Catalyst Surfaces by High CO coverage. *Science* **2010**, *327*, 850−853.
(27) Vang, R. T.; Lægsgaard, E.; Besenbacher, F. Bridging the Pressure Gap in Model Systems for Heterogeneous Catalysis with High-Pressure Scanning Tunneling Microscopy. *Phys. Chem. Chem. Phys.* **2007**, *9*, 3460−3469.
(28) Herbschleb, C.; van der Tuijn, P.; Roobol, S.; Navarro, V.; Bakker, J.; Liu, Q.; Stoltz, D.; Cañas-Ventura, M.; Verdoes, G.; van Spronsen, M.; et al. The ReactorSTM: Atomically Resolved Scanning Tunneling Microscopy under High-Pressure, High-Temperature Catalytic Reaction Conditions. *Rev. Sci. Instrum.* **2014**, *85*, 083703.
(29) Surface Preparation Laboratory, https://www.spl.eu/, consulted 2018-1-29.
(30) This is due to the factory preparation conditions of CH_3SH and not to the equilibration reaction.
(31) Kresse, G.; Joubert, D. From Ultrasoft Pseudopotentials to the Projector Augmented-Wave Method. *Phys. Rev. B: Condens. Matter Mater. Phys.* **1999**, *59*, 1758−1775.
(32) Kresse, G.; Hafner, J. *Ab Initio* Molecular Dynamics for Liquid Metals. *Phys. Rev. B: Condens. Matter Mater. Phys.* **1993**, *47*, 558−561.
(33) Kresse, G.; Hafner, J. *Ab initio* Molecular-Dynamics Simulation of the Liquid-MetalAmorphous-Semiconductor Transition in Germanium. *Phys. Rev. B: Condens. Matter Mater. Phys.* **1994**, *49*, 14251−14269.
(34) Kresse, G.; Furthmüller, J. Efficiency of *Ab-Initio* Total Energy Calculations for Metals and Semiconductors Using a Plane-Wave Basis Set. *Comput. Mater. Sci.* **1996**, *6*, 15−50.
(35) Kresse, G.; Furthmüller, J. Efficient Iterative Schemes for *Ab Initio* Total-Energy Calculations Using a Plane-Wave Basis Set. *Phys. Rev. B: Condens. Matter Mater. Phys.* **1996**, *54*, 11169−11186.
(36) Perdew, J. P.; Burke, K.; Ernzerhof, M. Generalized Gradient Approximation Made Simple. *Phys. Rev. Lett.* **1996**, *77*, 3865−3868.
(37) Perdew, J. P.; Burke, K.; Ernzerhof, M. Erratum: Generalized Gradient Approximation Made Simple [Phys. Rev. Lett. 77, 3865 (1996)]. *Phys. Rev. Lett.* **1997**, *78*, 1396−1396.
(38) Steinmann, S. N.; Corminboeuf, C. Comprehensive Benchmarking of a Density-Dependent Dispersion Correction. *J. Chem. Theory Comput.* **2011**, *7*, 3567−3577.
(39) Gautier, S.; Steinmann, S. N.; Michel, C.; Fleurat-Lessard, P.; Sautet, P. Molecular Adsorption at Pt(111). How Accurate are DFT Functionals? *Phys. Chem. Chem. Phys.* **2015**, *17*, 28921−28930.
(40) Steinmann, S. N.; Sautet, P. Assessing a First-Principles Model of an Electrochemical Interface by Comparison with Experiment. *J. Phys. Chem. C* **2016**, *120*, 5619−5623.
(41) Monkhorst, H. J.; Pack, J. D. Special Points for Brillouin-Zone Integrations. *Phys. Rev. B* **1976**, *13*, 5188−5192.
(42) Poirier, G. E.; Pylant, E. D. The Self-Assembly Mechanism of Alkanethiols on Au (111). *Science* **1996**, *272*, 1145−1147.
(43) Tersoff, J.; Hamann, D. R. Theory and Application for the Scanning Tunneling Microscope. *Phys. Rev. Lett.* **1983**, *50*, 1998−2001.
(44) Tersoff, J.; Hamann, D. R. Theory of the Scanning Tunneling Microscope. *Phys. Rev. B: Condens. Matter Mater. Phys.* **1985**, *31*, 805−813.
(45) Lorente, N.; Persson, M. Theory of Single Molecule Vibrational Spectroscopy and Microscopy. *Phys. Rev. Lett.* **2000**, *85*, 2997−3000.
(46) Tang, L.; Li, F.; Zhou, W.; Guo, Q. The Structure of Methylthiolate and Ethylthiolate Monolayers on Au(111): Absence of the $(\sqrt{3} \times \sqrt{3})$R30° Phase. *Surf. Sci.* **2012**, *606*, L31−L35.
(47) Kondoh, H.; Nozoye, H. Low-Temperature Ordered Phase of Methylthiolate Monolayers on Au(111). *J. Phys. Chem. B* **1999**, *103*, 2585−2588.
(48) Maksymovych, P.; Voznyy, O.; Dougherty, D. B.; Sorescu, D. C.; Yates, J. T. Gold Adatom as a Key Structural Component in Self-Assembled Monolayers of Organosulfur Molecules on Au(111). *Prog. Surf. Sci.* **2010**, *85*, 206−240.
(49) Torrelles, X.; Pensa, E.; Cortés, E.; Salvarezza, R.; Carro, P.; Guerrero, C. H.; Ocal, C.; Barrena, E.; Ferrer, S. Solving the Long-

DOI: 10.1021/acs.jpcc.9b03045
J. Phys. Chem. C 2019, 123, 12382−12389

Standing Controversy of Long-Chain Alkanethiols Surface Structure on Au(111). *J. Phys. Chem. C* **2018**, *122*, 3893−3902.
(50) Liao, S.; Shnidman, Y.; Ulman, A. Adsorption Kinetics of Rigid 4-Mercaptobiphenyls on Gold. *J. Am. Chem. Soc.* **2000**, *122*, 3688−3694.

DOI: 10.1021/acs.jpcc.9b03045
J. Phys. Chem. C 2019, 123, 12382−12389